J Mater Sci (2009) 44:1834–1843
DOI 10.1007/s10853-008-3230-9

Coolant pH control for optimum ceramic grinding. III. Rebinder Effect in silicon nitride

David W. Alley · Owen F. Devereux

Received: 3 August 2008 / Accepted: 29 December 2008 / Published online: 3 February 2009

Abstract The Rebinder Effect, an environment-caused change in the hardness of rock, ceramic, or glass, was investigated in silicon nitride using conventional microhardness and electrochemical techniques. As in previous studies of the effect, hardness and zeta potential varied significantly with the pH of the environment. Unlike previous studies, the pH values at which hardness was maximum and zeta potential was zero (zero point of charge, or zpc) did not correspond. This lack of correspondence was deemed the result of the partial oxidation of the surface film of the sample. The presence of the oxide containing film had a significant effect on zeta potential but little effect on hardness as the hardness indenter penetrated well beyond the film. Through the use of a simple linear model and published data it was possible to demonstrate that for oxide-free silicon nitride the pH values at which hardness was maximum and zeta potential was zero do correspond. The Rebinder Effect in this material is clearly time-dependent; long dwell times resulted in reduced hardness values. This was more noticeable at pH values removed from the zpc. These observations are consistent with a mechanism for the Rebinder Effect in which environmental pH controls surface charge, which in turn controls zeta potential and affects dislocation motion and, thereby, hardness.

D. W. Alley (✉)
Clearwater Systems Corp, 145 Denison Rd, Essex, CT 06426, USA
e-mail: dwa@clearwater-dolphin.com

O. F. Devereux
Department of Metallurgy and Materials Engineering, University of Connecticut, Storrs, CT 06269, USA

Introduction

The phenomenon known as the "Rebinder Effect" was discovered in 1928 by Rebinder [1, 2] (alternately Rehbinder) who found an anomalous softening of rock associated with the environment to which it was exposed. Rebinder attributed this softening to an adsorption-caused reduction in the surface free energy of the material and attempted to use the effect to reduce the energy required to drill oil wells. While successful on a laboratory scale, improvements in drilling efficiency were not significant in field operations. Work on the Rebinder Effect continued within the Soviet Union/Russia by colleagues of Rebinder, particularly Shchukin [3].

Interest in the Rebinder Effect outside the Soviet Union was revived in the 1960s and 70s by Westwood and others who extended the study of the Rebinder Effect to include not only rock, but ceramics [4–7] and glasses [4, 8, 9] as well. This work demonstrated that the environment could cause an *increase* in hardness as well as a decrease. The explanation of these findings required an expansion of Rebinder's theories because positive adsorption of a substance on a surface can only cause a reduction in surface free energy and, according to Rebinder's theory, a reduction in hardness [2] (Westwood did not appear to consider negative adsorption, i.e., near surface concentrations of species which are lower than the bulk concentration, which would cause an increase in surface free energy.). Based on work with CaF [6, 10], MgO [5, 7, 10], and ZnO [11], Westwood proposed that the environment affects the charge at the surface of the material which, in turn, affects dislocation mobility and, therefore, hardness. It should be noted that Westwood's explanation for the Rebinder Effect is not universally accepted. Alternate explanations involving hydrogen embrittlement [8], water content [12],

coefficients of friction [13], and changes in the properties of the diamond indenter or drill bit rather than the substrate [14], have been proposed and are supported by specific data sets. Additional papers by Westwood [15, 16], Macmillan [17], and Czernuszka and Page [18] provide reviews and insights into the subject.

Not withstanding the findings of Hainsworth and Page [19] regarding the desirability of using nanoindentation techniques for studies of this nature due to the small magnitude of the effect being measured as well as the reduced potential for operator bias, this study and its predecessors [20, 21] utilized microhardness measurement equipment and industrial quality surface grinders. While the use of state of the art research instruments may have provided more precise data, their use was strictly counter to one of the objectives of this work, i.e., to demonstrate that the Rebinder Effect can be a useful tool in improving the process of machining ceramic components using equipment consistent with current manufacturing technology.

The potential for operator bias to influence the results of these studies, as expressed by Hainsworth and Page [19], was recognized prior to the commencement of any work. Procedures were established and preliminary studies were conducted to minimize operator bias and to statistically establish the repeatabilities and uncertainties in the experimental techniques employed [20, 21].

Part I of this study [20] established that the Rebinder Effect in polycrystalline aluminum oxide could be observed using conventional equipment. Part II of this study demonstrated that the Rebinder Effect can be used to improve the process of grinding aluminum oxide parts on a commercial scale while using commercial equipment. This part of the study will demonstrate that not only is the Rebinder Effect observable in oxide materials, it is also present in silicon nitride. Silicon nitride was selected for this work due to its high ductility relative to other ceramic materials and, thereby, its commercial potential.

Experimental procedure

Material investigated and sample preparation

The material investigated was an experimental silicon nitride obtained from an industrial collaborator. It is not available commercially. The material was formed directly as a bulk solid via a vapor phase process without the need for sintering or sintering aides. It was selected for this study for its purity, low bulk oxygen content, and uniformity of composition between grains and grain boundaries. Samples were hot mounted and metallographically polished to a finish resulting from 1 μm diamond slurry. Following each polishing step, samples were ultrasonically cleaned in distilled water to ensure that no material other than water was entrapped in the sample or chemically or physically adsorbed on its surface.

Hardness measurements

Two series of Knoop hardness measurements were conducted. The first series of measurements was to determine the effect of environmental pH on hardness and, as will be discussed below, zeta potential. These measurements were made using a Leco (St. Joseph MI) DM-400FT microhardness tester with a load of 100 g and a dwell time of 10 s. The environment used for this series of experiments was distilled water adjusted for pH using NaOH and, as necessary, HNO_3. To ensure uniformity during the indenting process, several drops of the pH adjusted water were placed on the sample after it had been mounted in the hardness tester. A series of 13 indents were then made through the water. Between each indent, the stage of the harness tester was moved sufficiently to ensure the independence of the stress fields of each indent. Following the completion of all 13 indents, the sample was dried and 10 of the indents were measured using the optics of the microhardness tester. The "extra" indents were necessary as the "make all indents prior to measuring" strategy employed precluded the precise positioning of each indent and resulted in some interactions between indents and surface flaws. Such indents were, of course, not included in the reported data. This procedure was repeated on a second day in another area of the same sample. The values and statistics reported in the section "Results" below are based on the 20 measured indents.

The second series of measurements was made primarily to determine the effect of dwell time on hardness but is also relevant to the effect of pH on hardness. These measurements were made using a Leitz (Wetzler, Germany) Miniload hardness tester with a load of 200 g and dwell times of 10 s and 10 min. The Leitz instrument was used for this test series as the dwell time on the Leco instrument was automatically controlled with a maximum of 53 s. The environments used for this series of experiments were commercial buffer solutions ranging in pH from 4 to 10. Buffer solutions were used in this test series to minimize change in the pH of the environment during the experiment due to adsorption of CO_2 from the air. The composition of the buffer solutions used is listed in Table 1. The 200 g load was selected for this test series following preliminary tests with loads ranging from 100 to 500 g. The 200 g load produced less scatter in the data under the conditions tested than the other loads. Indentation procedures were similar to those employed during the first series although the number of usable indents varied with pH and dwell time (max 25, min 7).

Table 1 Buffer solution compositions

pH	Component	Concentration (wt%)
4	Potassium biphthalate	1.0
5	Potassium biphthalate	1.0
	Sodium hydroxide	0.1
6	Potassium phosphate monobasic	0.7
	Sodium hydroxide	0.02
7	Potassium phosphate monobasic	0.7
	Sodium hydroxide	0.1
9	Boric acid	0.3
	Potassium chloride	0.4
	Sodium hydroxide	0.1
10	Potassium carbonate	0.6
	Potassium borate	0.2
	Potassium hydroxide	0.4

The uncertainties shown in the figures were determined by a statistical analysis (Student's T test) and give the 90% probability range for the mean. This uncertainty includes the fixed uncertainties of the optical system as well as the uncertainties introduced by the operator and the actual variability of the hardness of the material.

Electrochemical measurements

The electrochemical parameter of interest in this study of the Rebinder Effect is surface charge, specifically the combination of test material, silicon nitride in this case, and environmental conditions which result in a surface charge of zero. In most systems, including the present system, surface charge cannot be directly measured or calculated. As set forth below, surface charge is related to the zeta potential which may be calculated from measurements of an electrokinetic phenomenon known as the streaming potential.

The distribution of potential in the vicinity of the interface separating two immiscible phases may be relatively simple or quite complex. In its most simple form, two layers of charge, one negative and one positive, i.e., an electrical double layer, are considered to exist. In the case of a ceramic immersed in a dilute ionic solution, typified by Fig. 1, as many as four layers may be present: the ceramic surface, a layer of chemically adsorbed ions, the compact layer, and the diffuse layer. Chemically adsorbed ions are sometimes represented as being part of the ceramic surface. Despite the increased complexity of the near surface region of this system, the term "double layer" is still employed.

Again considering Fig. 1, if a mechanical force is applied to the ionic fluid to cause a flow of the fluid into the page, a competition will be established between electrical and mechanical forces. At large distances from the surface

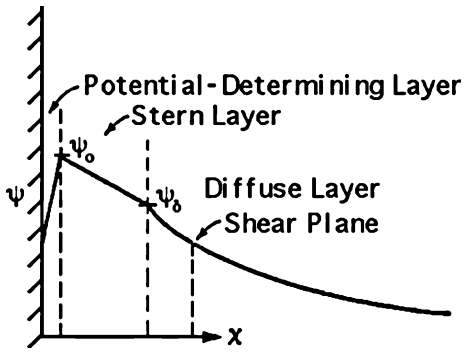

Fig. 1 Electrical double layer

the mechanical forces will prevail and fluid will flow into the page. Some charge will be carried with the flowing fluid. Close to the charged surface, electrical forces will prevail and the fluid will remain fixed. The plane representing the boundary between flowing and non-flowing fluid, the shear plane, is shown within the diffuse layer in Fig. 1. The potential at the shear plane is known as the zeta potential (ζ).

While the distance between the ceramic surface and the shear plane is not known and cannot be determined, the zeta potential can be readily calculated from measurements of the streaming potential. The streaming potential is the potential difference between electrodes placed upstream and downstream of a surface over which an electrolyte is flowing. The streaming potential is the electrical potential necessary to offset the mechanical transport of ions outside of the shear plane, i.e., the streaming potential is that potential at which the rate of transport of ions outside of the shear plane in the downstream direction due to mechanical forces is balanced by the transport of ions upstream due to the electrical potential difference. The zeta potential is related to the streaming potential by

$$\zeta = \frac{4\pi E \mu k}{PDD_0} \tag{1}$$

where

E = Measured streaming potential (V)
μ = Viscosity (cP)
k = Conductivity of the electrolyte ($\mathrm{Ohm}^{-1}\ \mathrm{cm}^{-1}$)
P = Pressure drop ($\mathrm{dyn/cm}^2$)
D = Relative dielectric constant of the electrolyte
D_0 = Dielectric constant of a vacuum (1.112×10^{-10} $\mathrm{C}^2/\mathrm{N\ m}^2$)

For a simple "Gouy-Chapman" double layer [22], comprised only of a charged surface and a diffuse layer containing a balancing charge, the apparent surface charge, η, is related to the potential measured at any distance from the surface within the double layer by

$$\eta = \frac{DD_0\kappa\psi_x e^{\kappa x}}{4\pi} \quad (2)$$

where

η = Charge density, charge/unit area (C/m^2)
D = Relative dielectric constant of the electrolyte
D_0 = Dielectric constant of a vacuum
(1.112×10^{-10} C^2/N m^2)
κ = Constant, $1/\kappa$ is half the thickness of the diffuse layer (m^{-1})
x = Distance measured from the surface (m)
ψ_x = Potential at a distance x from the surface (V)

If the distance between the ceramic surface and the shear plane were known it would be a relatively simple matter to substitute ζ for ψ_x and calculate the surface charge. Lack of knowledge of this distance precludes calculation of the surface charge for most conditions. It may, however, be seen that the surface charge must be zero when the zeta potential is zero and that for other values of the zeta potential there is a monotonic relationship between the zeta potential and surface charge [22]. Use of Eq. 2 is limited further by the assumptions inherent in the Gouy-Chapman treatment of the double layer. Of particular significance to this investigation is the requirement that the ionic solution be dilute, typically 10^{-3} for aqueous solutions at 25 °C.

In this case, the charged surface was a packed bed of crushed Si_3N_4 made from the same batch of material used in the indentation tests. Maximum particle size was 1 mm; fines created by crushing were not removed. Streaming potentials were measured with the apparatus schematically represented in Fig. 2. The packed column was approximately 20 cm long by 6 mm diameter and the hydrostatic head was of the order of 3 m. Flow rates through the apparatus of approximately 3-5 drops per second produced stable and consistent streaming potential values. In this case the tube containing the packed bed was Pyrex® which is predominantly silica. Given the high surface area of the bed in comparison to the tube, the contribution of the tube to the measured streaming potential was neglected. The electrodes were lengths of type 316 stainless steel tubing loosely packed with stainless steel ribbon.

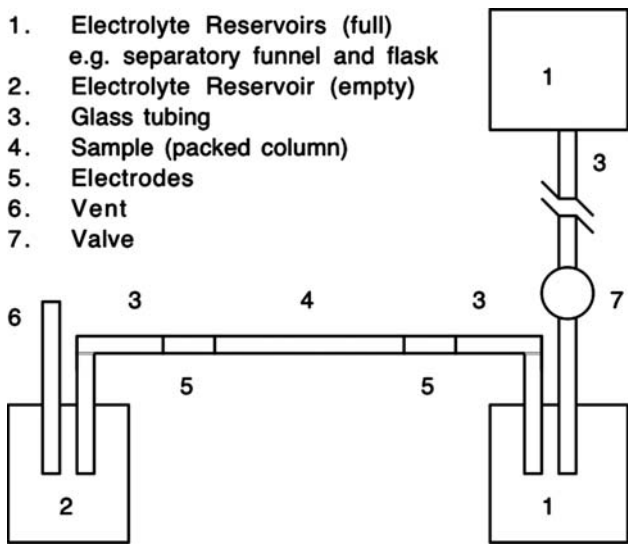

Fig. 2 Schematic of streaming potential measurement apparatus

Streaming potential measurements were made by filling the test apparatus with a solution of the desired pH and allowing 100–200 mL to pass through the packed column to rinse it. The flow was stopped and an electrometer was then connected to the electrodes. The system was allowed to stabilize so that the drift in measured potential difference was less than 0.1 mV/s. The electrometer never stabilized at 0 V. The flow was re-initiated, producing a rapid change in potential difference followed, in a few seconds, by a period of markedly reduced change. The streaming potential was defined as the difference between the potential difference when the valve is opened and the potential difference when the rate of change of the potential difference dramatically slowed, i.e., began to drift as previously described [22–24].

Results

Figure 3 shows the relationship between pH and hardness for environments of pH controlled distilled water. It may be seen that the hardness reaches a maximum at pH 10.5. If the hardness measured at pH 4 and 5 is assumed to be the "baseline" hardness, the hardness at all other pH values is statistically different from this baseline at a confidence level of 90% (Student's T test). The hardness values measured at pH 4 and 5 were selected as the baseline

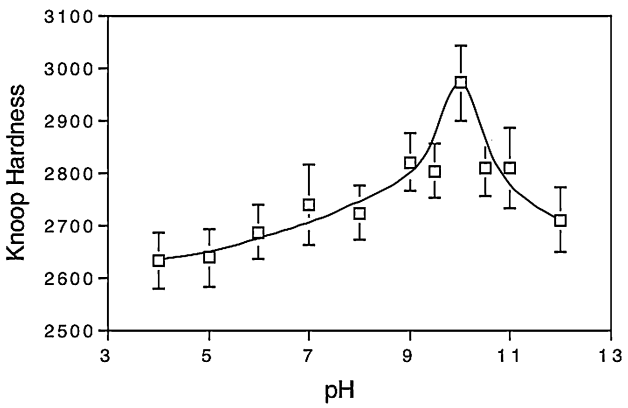

Fig. 3 Variation in hardness with pH. Silicon nitride in pH controlled distilled water. Dwell time = 10 s. Error bar represents 90% confidence for the mean

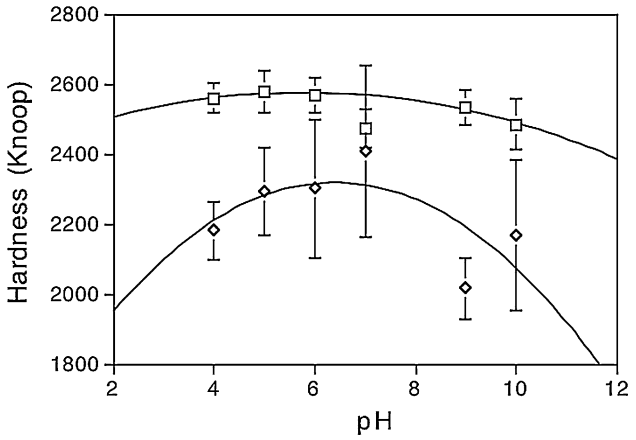

Fig. 4 Variation in hardness of silicon nitride with pH and dwell time. Upper curve dwell time = 10 s, lower curve dwell time = 10 min. Commercial buffer solutions, see Table 1. Error bar represents 90% confidence for the mean

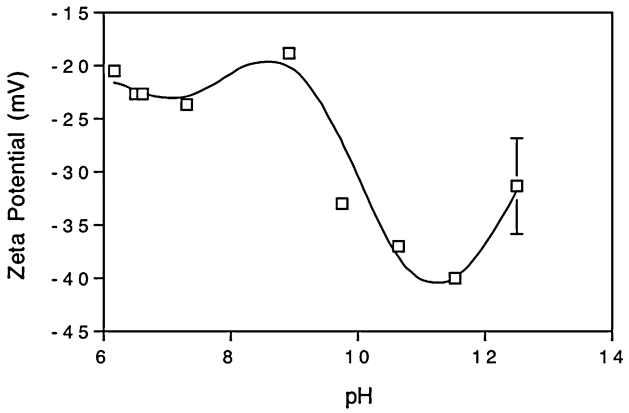

Fig. 5 Variation in zeta potential with pH. Silicon nitride in pH controlled distilled water. Error bar represents 90% confidence for the mean. Error bars of all data points other than pH 12.5 are smaller that the data symbol

values because it appears that hardness is relatively insensitive to pH at these and more acidic values of pH.

Figure 4 shows the relationships between pH, hardness, and dwell time for environments of commercial buffer solutions. This figure illustrates that, as in Fig. 3, there is a pH at which maximum hardness occurs. For both the 10 s and 10 min dwell time the pH corresponding to maximum hardness is pH 6. This shift in the pH of maximum hardness between Figs. 3 and 4 is related to the ionic composition of the buffer solutions as compared to the sodium hydroxide solution used in Fig. 3. This issue is further addressed in the section "Discussion". Additionally, Fig. 4 demonstrates that longer dwell times result in a general softening of the material. The softening effect, i.e., the difference in hardness between the short dwell time and the long dwell time, is more pronounced at pH values away from the pH at which maximum hardness is observed. It should be noted that the second order curve used to fit the 10 s indent data and, therefore, the maximum in that data at pH 6 are based on trends found both in this work and preceding works [20, 21]. One could also draw a zero order (horizontal) line through the data which would correspond to no correlation between pH and hardness at indent times of 10 s or less.

Figure 5 illustrates the relationship between pH and zeta potential for an environment of pH adjusted distilled water. Of significance in this figure is the marked change in zeta potential in the vicinity of pH 10.5, the pH of maximum hardness in pH adjusted distilled water. As will be addressed in the section "Discussion", the observations shown in this figure suggest that silica (SiO_2) was present and made a significant contribution to the electrical behavior of the sample.

Figure 6 shows the variation of the chemical composition of an as-prepared silicon nitride specimen with

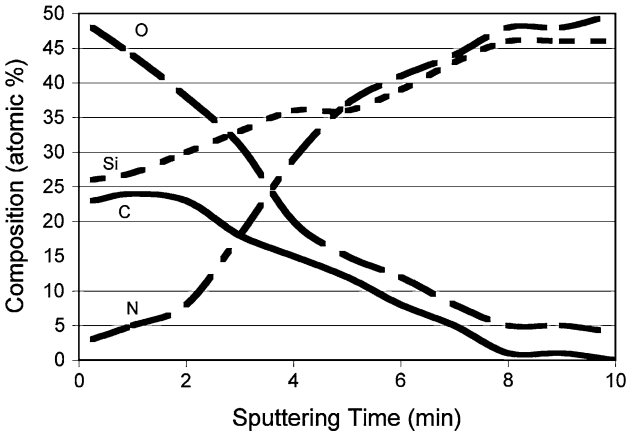

Fig. 6 Variation in chemical composition of silicon nitride test specimen with depth from surface as determined by XPS. Based on silica, penetration is 740 Å/min

distance from the surface of the sample (sputtering time) as determined by XPS (X-ray photoelectron spectroscopy). These data were obtained by a Quantum 2000 scanning ESCA microprobe (Physical Electronics, Chanhassen, MN). Sputtering was conducted on a 0.25 min cycle using a 4 kV argon ion beam over a 2 × 2 mm^2 area. Spectra were collected using a 200 μm X-ray beam and a 29.35 eV pass energy over the Si2p, C1s, O1s, and N1s regions. Based on silica, the sputtering rate is 740 Å/min. From this figure it may be seen that a substantial amount of carbon is present at the surface of the sample. In the near surface region oxygen is present in substantial quantities and nitrogen is substantially absent. Oxygen decreases with depth and nitrogen increases with depth until, at about 9 min sputtering time, oxygen is essentially absent.

Figure 7 shows the variation in mole percentages of the expected compounds in the near surface region of the

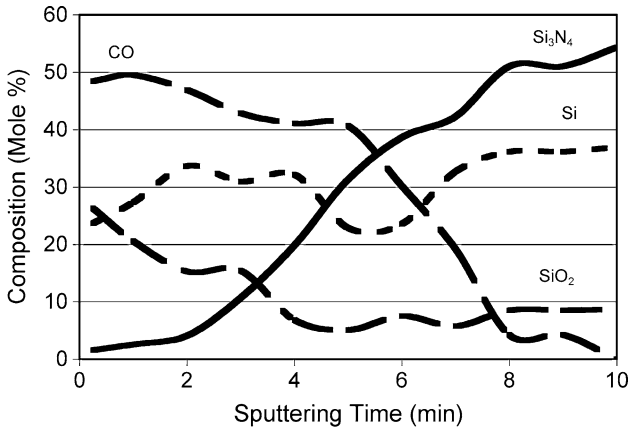

Fig. 7 Proposed variation of molecular composition of silicon nitride test specimen with depth from surface as determined by XPS. Based on silica, penetration is 740 Å/min

sample. This figure assumes that all nitrogen is bonded to silicon. It then assumes that sufficient oxygen is bonded to the carbon to form carbon monoxide. The remaining oxygen is assumed to be bonded to silicon as silicon dioxide. Any remaining silicon is assumed to be present as elemental silicon. From this figure it may be seen that the surface of the sample is primarily carbon monoxide and silicon dioxide. While a substantial concentration of elemental silicon is shown in the figure, it is believed that this is due to either an artifact in the model or a slight error in the measured concentration of oxygen or silicon in the near surface region. As sputtering time increases the concentration of silicon nitride increases while the concentrations of carbon monoxide and silicon dioxide decrease.

Figure 8 is an alternate approach to considering the data of Fig. 6. Figure 8 considers the percentage of silicon atoms present in the sample which are present as silicon nitride, silicon dioxide, or as elemental silicon. Carbon, and

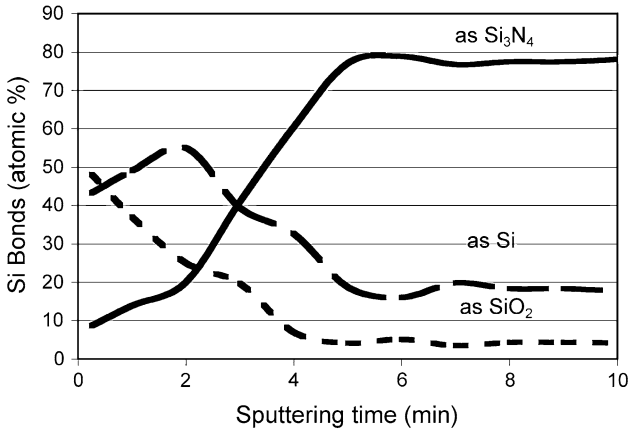

Fig. 8 Proposed variation of silicon atoms bonded as Si_3N_4, SiO_2, or elemental Si of silicon nitride test specimen with depth from surface as determined by XPS. Based on silica, penetration is 740 Å/min

the oxygen associated with it are not considered in this figure. From this figure it may be seen that at the surface most of the silicon is present as either elemental silicon or as silicon dioxide. As in Fig. 7 it is believed that the relatively high concentration of elemental silicon at the surface is due to either an artifact in the model or a slight error in the measurement of either the oxygen or silicon in the near surface region. The percentage of silicon present as silicon nitride increases with depth such that after about 5 min of sputtering steady concentrations of silicon nitride (78%), silicon dioxide (4%), and elemental silicon (18%) are reached.

Discussion

Prior to considering the implications of the observation of the Rebinder Effect in silicon nitride, it may be beneficial to briefly review similar results obtained for aluminum oxide [20]. Figure 9 shows the effect of pH on the hardness and zeta potential of polycrystalline aluminum oxide in a solution of pH adjusted distilled water. This figure illustrates that hardness and zeta potential of the aluminum oxide vary with pH and that maximum hardness and zero zeta potential occur at the same pH.

Figure 10 shows the effect of pH on the hardness and zeta potential for polycrystalline aluminum oxide when exposed to commercial buffer solutions. This figure, like Fig. 9, shows that hardness and zeta potential vary with pH and that maximum hardness and zero zeta potential occur

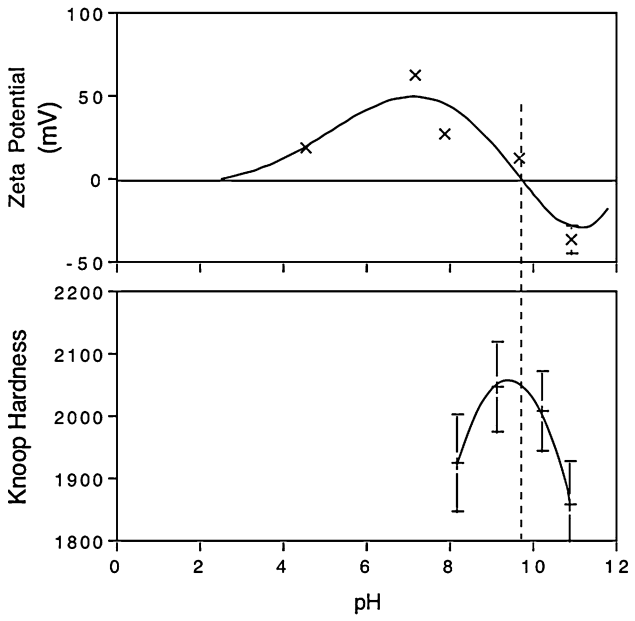

Fig. 9 Variation of zeta potential (**a**) and Knoop hardness (**b**) with pH. Polycrystalline aluminum oxide in pH controlled distilled water. Error bar represents 90% confidence for the mean

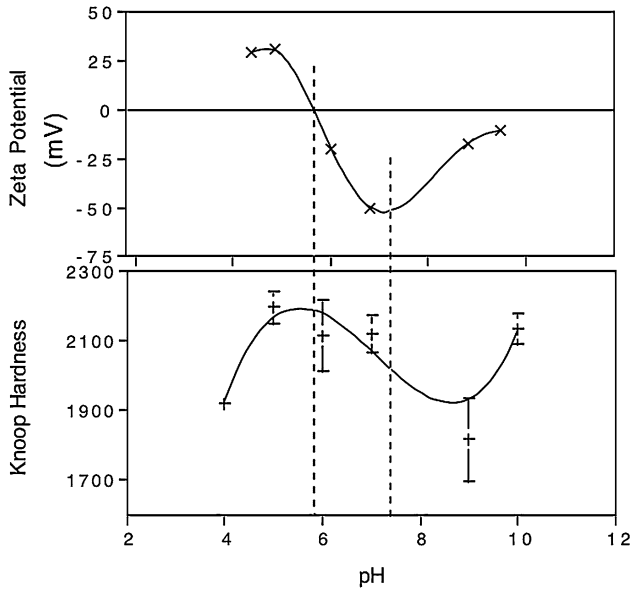

Fig. 10 Variation of zeta potential and hardness of polycrystalline aluminum oxide with pH in commercial buffer solutions. Error bar represents 90% confidence for the mean. The error bar for the first data point in graph b is smaller than the symbol for that point and is, therefore, not visible

at the same pH (left hand vertical dashed line in the figure). In addition, Fig. 10 shows a moderate correlation between a maximum in the absolute value of the zeta potential and a minimum in the hardness (right hand vertical dashed line in the figure).

Westwood [15] attributed findings of this nature to the effect of surface charge on dislocation motion. The type and extent of material chemisorbed on a surface alters the electronic state of near surface point defects and dislocations, which, in turn, varies their mutual interactions and, thereby, their mobility. At zero surface charge dislocation motion is restricted and hardness is maximum. When surface charge is not zero, whether it is positive or negative, dislocations move more readily and hardness is reduced. This mechanism of the Rebinder Effect implies that hardness should be inversely related to indenter dwell time as has been previously found for single crystals CaF_2, MgO, and Al_2O_3 [7, 10, 12]. We did not observe this time dependency on hardness with polycrystalline Al_2O_3 [20]. This apparent contradiction may or may not be significant as the relatively short range of dwell times investigated and the relatively short path available for dislocation motion within a single Al_2O_3 grain may have masked any time dependence of the hardness measurements. It is, however, also possible that some non-time dependent plastic deformation mechanism, such as twinning, which is known to occur in Al_2O_3 at room temperature, may have been responsible for variations in hardness.

It is interesting to compare the effects of pH adjusted water and commercial buffer solutions on hardness and zeta potential. Based on the similarity of the magnitudes of the zeta potentials and the shape of the fitted curves in Figs. 9 and 10, it appears that the anions in the buffer solution caused the zeta potential versus pH curve to shift in the acidic direction by approximately four pH units. While it is expected that zeta potential would depend on pH (surface potential is determined by the competition of H^+ and OH^- ions for adsorption sites) [25], it is not completely obvious that all anions used in commercial buffer ions should have the same effect, i.e., cause the same shift in the zero of the zeta potential. This similarity in effect appears to be due to the structure of the anions. Most of the anions consist of a small cation surrounded by one or more oxygen atoms. For commercial buffer solutions, the primary zeta potential controlling interaction, irrespective of the anion present, is between the surface and oxygen atoms in the anions.

As will be seen below, manipulation of the zeta potential curves is required to fully interpret the results of this work. This requires some knowledge of the relationship between zeta potential and surface charge as well as of the general shape of the zeta potential curve. If the assumptions for the Gouy-Chapman analysis of the double layer are valid, the surface charge is related to the surface potential and thereby the zeta potential by

$$\eta_0 = -\sqrt{\frac{DD_0kTn_0}{2\pi}}\sqrt{2\left(\cosh\left(\frac{z\varepsilon\psi^0}{kT}\right)-1\right)} \tag{3}$$

where

η_0 = Surface charge density (charge/area) (C/m^2)
n_0 = Ionic concentration beyond the double layer (m^{-3})
D = Relative dielectric constant of the electrolyte
D_0 = Dielectric constant of a vacuum (1.112×10^{-10} C^2/N m^2)
z = Ionization number
ε = Charge on an electron (-1.602×10^{-19} C)
ψ_0 = Surface electrical potential at the surface in question
k = Boltzmann's constant (1.3805×10^{-23} J/K)
T = Absolute temperature (K)

From Eqs. 2 and 3 it may be seen that when the surface charge is near zero, small changes in the charge will cause relatively large changes in the surface electrical potential and, therefore, in the zeta potential. As surface charge increases, changes in the charge make smaller changes in the surface and zeta potentials. Eventually, as a monolayer of ions forms on the surface, the surface potential and, therefore, the zeta potential reach a plateau.

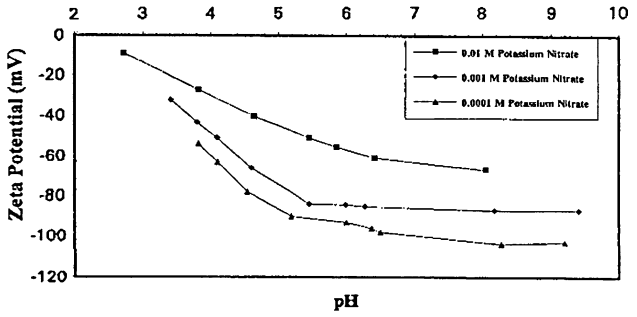

Fig. 11 Zeta potential versus pH for vitreous silica at varying electrolyte concentrations (after McFadyen [26])

These principles are illustrated in Fig. 11 for vitreous silica [26]. Near the zero point of the surface charge, which is also the zero point of the zeta potential, it may be seen that small changes in the potential determining species, in this case the H^+ ion (pH), result in large changes in zeta potential. At surface charges, and zeta potentials, far from the zero point, large changes in the potential determining species result in little if any change in zeta potential.

An additional aspect of Fig. 11 which merits consideration is that the zeta potential is affected by the overall ionic concentration in solution. While the overall ionic concentration does not affect the pH at which the zeta potential is zero (all three curves shown in Fig. 11 should cross the zero of the zeta potential at a pH of about 2.5), an increase in the ionic concentration causes a decrease in the absolute value of the zeta potential at all other values of pH. This decrease in zeta potential is attributed to a decrease in the thickness of the double layer. As may be seen in Fig. 12, for a fixed surface potential, the observed zeta potential decreases with overall solution concentration. The zeta potential will asymptotically approach zero as the thickness of the double layer approaches the location of the shear plane. Although there is no precise limit to the concentration of a solution for which the thinning of the double layer with increasing ionic concentration can be ignored, through much of his work

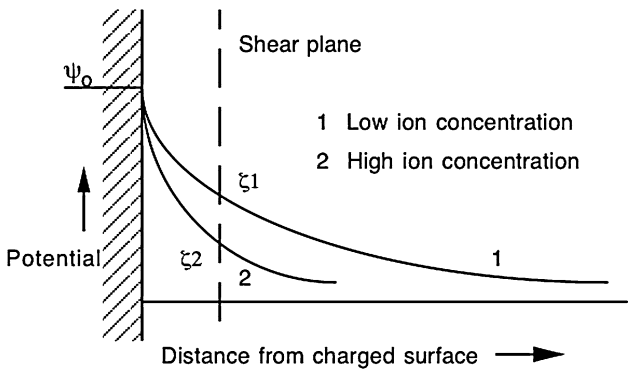

Fig. 12 Relationship between zeta potential and surface charge for varying ion concentration (after Kruyt [27])

Westwood has used solution concentrations in the 10^{-3}–10^{-6} molar range, apparently to avoid this phenomenon. When necessary, he has used solutions of approximately 1 molar to ensure that the zeta potential is zero irrespective of the surface charge [11]. The outgrowth of this analysis is that when ionic concentration does not exceed approximately 10^{-2} M, i.e., between approximately pH 2 and pH 12, the zeta potential may be idealized as two horizontal plateaus, one positive and one negative joined by a sloping section containing zero surface charge and zero zeta potential. In Fig. 11 the positive plateau is off scale to the left. For pH values below 2 and above 12, the zeta potential, but not the surface potential or surface charge, asymptotically approaches zero.

Having characterized the Rebinder Effect in polycrystalline aluminum oxide, it is now possible to consider the Rebinder Effect in silicon nitride. In the light of the results for polycrystalline aluminum oxide, it was expected that a hardness maximum would also occur at the pH of zero zeta potential for silicon nitride. This was not the case. From Fig. 3 it may be seen that the hardness maximum for silicon nitride occurs at pH 10.5 in pH adjusted distilled water. Figure 5 shows that the zeta potential is not zero at pH 10.5 but rather is near a local maximum.

The apparent discrepancy between expectations for the zeta potential and hardness and the actual observations is addressed by Figs. 6, 7, and 8. These figures show that the surface of the sample is predominantly silicon dioxide. The concentration of silicon dioxide decreases with depth, approaching 0% at a depth of approximately 0.7 μm. It is reasonable to assume that the measured values for zeta potential and hardness will represent a mixture of values characteristic of pure silicon dioxide and pure silicon nitride and, therefore, that the zeta potential observed in these experiments reflects a surface which is high in, but not pure, silicon dioxide. The extent of the oxidation of the new surfaces generated by crushing the silicon nitride to the 1 mm particle size used in the streaming potential tests is likely to be similar to the surface of the polished sample which was subjected to XPS testing. Hardness tests, on the other hand, will more closely reflect the properties of silicon nitride as the hardness indent is deep compared to the thickness of the silicon dioxide surface layer.

As a first approximation, it is proposed that the measured zeta potential follows the law of mixtures, i.e.,

$$\zeta_m = x_s\zeta_o + (1 - x_s)\zeta_n \tag{4}$$

where

ζ_m = zeta potential, measured
ζ_o = zeta potential, silicon dioxide
ζ_n = zeta potential, silicon nitride
x_s = area fraction of silicon dioxide at the surface

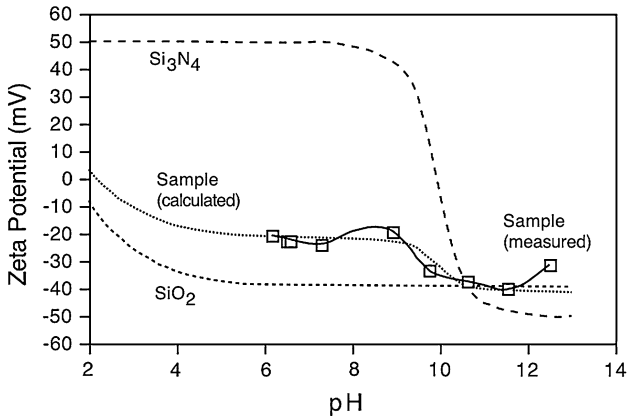

Fig. 13 Zeta potentials. Pure SiO_2 and pure Si_3N_4

If this assumption is valid, it should be possible to recreate an idealized version of the observed zeta potential curve (Fig. 5) using the properties of the zeta potential previously discussed and data for pure silicon dioxide and pure silicon nitride. Figure 13 shows the results of this effort. An area fraction, x_s, of 0.8 was used in Eq. 4 to model the zeta potential curve for the sample. Zeta potential curves for pure silicon nitride and pure silicon dioxide are based on typical values found in the literature. The silicon dioxide curve is based on Johnson and Parks [25, 28]. They report that the zero of the zeta potential occurs at approximately pH 2. Johnson [28] found that the plateau potential of the zeta potential varied between −10 and −52 mV. No data for pure silicon nitride were found. Most silicon nitride studied contained measurable amounts of silicon dioxide (used to facilitate the formation of bulk silicon nitride by sintering) or silicon carbide. Whitman and Fenke [29], Hackley [30], and Joshi [31] found that the zero of the zeta potential varied from pH 3 for silicon nitride samples containing high concentrations of silicon dioxide to nearly 9 for samples containing lower concentrations. Extrapolation of this trend suggests that the zero of the zeta potential of pure silicon nitride will occur at a pH greater than 9. Joshi [30] reported that the plateaus for the samples tested were ±40–50 mV. To best fit the experimental data, Fig. 13 is constructed using values of −38.75 mV for the silicon dioxide plateau, +50 mV and −50 mV for the silicon nitride plateaus, and a pH of 10 for the zero of the silicon nitride zeta potential.

We drew several inferences from Fig. 13. First, the surface region of typical bulk silicon nitride contains appreciable silicon dioxide and its zeta potential may be reasonably modeled as linear combination of the zeta potentials of silicon nitride and silicon dioxide. Second, as might be expected, the crushing of bulk silicon nitride followed by exposure to water resulted in substantial, but not complete, oxidation of the surface. Third, Fig. 13 helps to establish the zero of the zeta potential for pure silicon nitride at approximately pH 10, consistent with the values for mixed silicon nitride and silicon dioxide found in the literature. Lastly, Fig. 13, in combination with Fig. 3, suggest that the maximum in the hardness of the silicon nitride sample used in this work occurs at approximately pH 10 to 10.5, coincident with the zero of its zeta potential and consistent with predominant current concepts on the mechanism of the Rebinder Effect.

Figures 9 and 10 demonstrate that, for aluminum oxide, the use of commercial buffer solutions in place of pH-adjusted distilled water caused the pH at which maximum hardness is observed to shift in the acidic direction approximately 4 pH units, from approximately 9.5 to approximately 5.5. Figures 3 and 4 illustrate a similar shift from approximately pH 10.5 to pH 6.5 for silicon nitride. The rationale for such a shift is clearly related to the ionic composition of the buffer solutions [20] but as the chemistry of these solutions is different for each pH the shift of the hardness–pH curve is far more complex than a simple translation.

Prior work on a variety of materials (CaF_2, MgO, and Al_2O_3 [7, 10, 12]) indicated that hardness is not only a function of pH but also of indenter dwell time. Hardness values measured at long dwell times were found to be less than those measured at short dwell times. It was proposed that the Rebinder Effect was the result of changes in the ease of motion of dislocations as the result of changes in surface charge. Zero zeta potential caused decreased dislocation mobility while zeta potentials with greater absolute values allowed greater dislocation mobility and reduced hardness. Figure 4 is supportive of that mechanism. First, all of the hardness values measured at short dwell times are greater than those measured at long dwell times, i.e., the penetration of the indenter is governed by a time dependent mechanism, such as dislocation motion. Second, a maximum in the measured hardness values exists at approximately pH 6.5 for both the long and short indents, i.e., the pH of zero surface charge. As we move further from this pH the magnitude of the charge at the surface increases, increasing (by postulate) dislocation mobility and reducing measured hardness. Lastly, the difference in hardness between long and short dwell times is greater at pH values where the measured hardness is lower. At the zero point of charge, where dislocation motion is difficult, a short dwell time will result in a small indent (hard surface). Additional dwell time will result in very little indent enlargement and very little apparent softening of the surface. Conversely, at pH values away from the zero point of charge, where dislocation motion is comparatively easy, a short dwell time will result in a large indent (soft surface). Additional dwell time will permit continued rapid dislocation motion and will result in

considerable indent enlargement and significant apparent softening of the surface.

It should be noted that, while ductility and dislocation motion are not normally associated with silicon nitride, both effects have been observed. Ductile behavior has been observed in silicon nitride undergoing single point machining [32]. Dislocation motion has been observed in silicon nitride undergoing wear testing [33]. These results indicate a possibility that the mechanism for the Rebinder Effect in silicon nitride is similar to that proposed for other materials.

Conclusions

The Rebinder Effect has been investigated in high-purity silicon nitride using conventional methods for measuring microhardness and zeta potential. The presence of the Rebinder Effect in this material in aqueous solutions of various pH values was confirmed at a confidence of greater than 90% (Student's T test). The investigation was complicated to some extent by the tendency of the surface of the silicon nitride sample to oxidize which affected the zeta potential. A linear model using the zeta potential values of silicon dioxide and silicon nitride was effective in representing the measured zeta potential curve of the sample permitting estimation of the zero zeta potential for pure silicon nitride. Hardness measurements, due to their depth, reflected the bulk composition (essentially pure silicon nitride) of the material. For environments consisting of pH adjusted distilled water, maximum hardness and zero zeta potential estimates of pure silicon nitride occurred simultaneously at pH 10 to 10.5.

Maximum hardness for silicon nitride tested in environments of commercial buffer solutions at long (10 min) and short (10 s) dwell times occurred at pH 6.5. This represents a shift in the pH of the maximum hardness in the acidic direction by 4 pH units. This is expected, and in all likelihood is attributable to anion adsorption on the surface. The anions are all essentially a cluster of oxygen atoms polarized by a small cation whose identity is different for each pH.

Increased dwell time was observed to result in reduced measured hardness. This effect was most prominent at pH values where the sample was softest. These observations are consistent with a mechanism for the Rebinder Effect in which surface charge affects dislocation mobility.

Acknowledgements The authors wish to acknowledge the contributions of Norma Kahn (UOP LLC, Des Plaines, IL) and Gregory Alley (Harper College, Palatine, IL) for their contributions to data acquisition (XPS and hardness measurements for buffered solutions) for this work.

References

1. Rebinder PA (1928) In: Proc 6th Physics Conf, Moscow
2. Rebinder PA et al (1948) Hardness reducers in rock drilling. C.S.I.R.O, Melbourne, Australia
3. Shchukin ED (2006) Adv Colloid Interface Sci 123–126:33
4. Westwood ARC, Latanision RM (1972) The science of ceramic machining and surface finishing. NBS Special Pub 348, U.S. Government Printing Office, Washington DC, p 141
5. Burnett PJ, Page TF (1985) J Mater Sci Lett 4:1364
6. Westwood ARC, Goldheim DL (1968) J Appl Phys 49(7):3401
7. Westwood ARC, Goldheim DL, Lye RG (1967) Philos Mag 16:505
8. Cuthrell RE (1978) J Appl Phys 49(1):432
9. Michalske TA, Bunker BC (1987) Sci Am 257:122
10. Westwood ARC, Goldheim DL (1970) J Am Ceram Soc 53(3):142
11. Ahearn JS, Mills JJ, Westwood ARC (1979) J Phys 40:c6
12. Westbrook JH, Jorgensen PJ (1965) Trans AIME 233(2):425
13. Hanneman RE, Westbrook JH (1968) Philos Mag 18:73
14. Cooper GA (1979) The science of ceramic machining and surface finishing II. NBS Special Pub 562, U.S. Government Printing Office, Washington DC, p 115
15. Westwood ARC, Ahearn JS, Mills JJ (1981) Colloids Surf 2:1
16. Westwood ARC, Mills JJ (1977) In: Latanision RM, Fourie JT (eds) Proceedings of the NATO advanced study institute on surface effects in crystal plasticity, Hohegeiss, Germany, September 1975. Noordhoff, Leyden, The Netherlands, p 835
17. Macmillan NH (1977) In: Latanision RM, Fourie JT (eds) Proceedings of the NATO advanced study institute on surface effects in crystal plasticity, Hohegeiss, Germany, September 1975. Noordhoff, Leyden, The Netherlands, p 629
18. Czernuszka JT, Page TF (1987) J Mater Sci 22:3917. doi: 10.1007/BF01133340
19. Hainsworth SV, Page TF (1994) J Mater Sci 29:5529. doi: 10.1007/BF00349944
20. Alley DW, Devereux OF (2002) J Mater Sci 37:5135. doi:10.1023/A:1021072607565
21. Alley DW, Devereux OF (2003) J Mater Sci 38:1353. doi: 10.1023/A:1022819517624
22. Graham DC (1947) Chem Rev 41:441
23. Adamson AW (1976) Physical chemistry of surfaces. Wiley Interscience, New York, NY, p 196
24. Zucker GL (1959) A critical evaluation of streaming potential measurements. Columbia University, Eng. Sc. D. p 36
25. Parks GA (1965) Chem Rev 65:177
26. McFadyen P, Fairhurst D (1993) Proc Br Ceram Soc 51:175
27. Kruyt HR (1952) Colloid science, vol 1. Elsevier Publishing Co, Houston, TX
28. Johnson PR (1996) Environ Sci Technol 30:3284
29. Whitman PK, Feke DL (1988) J Am Ceram Soc 71(12):1086
30. Hackley VA (1977) J Am Ceram Soc 80:2315
31. Joshi PN, Mccauley RA (1994) J Am Ceram Soc 77:2926
32. Kumbera TG et al (2001) In: Proceedings of 4th CIRP internation workshop on modeling of machining operations, p 7
33. Zutshi A et al (1994) J Am Ceram Soc 77(4):883